

A Model of H-NS Mediated Compaction of Bacterial DNA

Marc Joyeux^{†*} and Jocelyne Vreede^{†*}

[†]Laboratoire Interdisciplinaire de Physique, Centre National de la Recherche Scientifique UMR5588, Université Joseph Fourier Grenoble 1, St. Martin d'Hères, France; and [†]Van't Hoff Institute for Molecular Sciences, University of Amsterdam, Amsterdam, The Netherlands

ABSTRACT The histone-like nucleoid structuring protein (H-NS) is a nucleoid-associated protein, which is involved in both gene regulation and DNA compaction. H-NS can bind to DNA in two different ways: in *trans*, by binding to two separate DNA duplexes, or in *cis*, by binding to different sites on the same duplex. Based on scanning force microscopy imaging and optical trap-driven unzipping assays, it has recently been suggested that DNA compaction may result from the antagonistic effects of H-NS binding to DNA in *trans* and *cis* configurations. To get more insight into the compaction mechanism, we constructed a coarse-grained model description of the compaction of bacterial DNA by H-NS. These simulations highlight the fact that DNA compaction indeed results from the subtle equilibrium between several competing factors, which include the deformation dynamics of the plasmid and the several binding modes of protein dimers to DNA, i.e., dangling configurations, *cis*- and *trans*-binding. In particular, the degree of compaction is extremely sensitive to the difference in binding energies of the *cis* and *trans* configurations. Our simulations also point out that the conformations of the DNA-protein complexes are significantly different in bulk and in planar conditions, suggesting that conformations observed on mica surfaces may differ significantly from those that prevail in living cells.

INTRODUCTION

The chromosomal DNA of bacteria is folded into a compact body, called the nucleoid, which is distinctly different from the rest of the cytoplasm. Bacteria employ a number of nucleoid-associated proteins that influence the organization of the nucleoid by bending, wrapping, or bridging DNA (1–4). In addition, most of these proteins act as global regulators of gene expression (5,6). The histone-like nucleoid structuring protein (H-NS) is a key player in genome organization by forming bridges between DNA duplexes (7,8). Moreover, H-NS is an important global regulator (regulating several hundreds of genes) and may function as an environmental sensor (9,10) that perceives changes in the growth conditions of the bacterium and facilitates physiological changes required for adaptation to the new conditions. H-NS is a small protein (137 residues, 15.5 kDa), which is functional as a dimer. Each monomer is composed of an N-terminal dimerization domain (residues 1–64) (11,12) connected to a C-terminal DNA-binding domain (residues 91–137) (13) through a flexible linker (14). The dimer can bind to DNA in two different ways, namely in *trans*, by binding to two separate DNA duplexes, and in *cis*, by binding to different sites on the same duplex (7,8,15,16). The contemporary view reflects that H-NS initially binds to specific nucleotide sequences (13,17), followed by additional H-NS dimers binding to adjacent sites on DNA (14,18).

Despite the enormous effort of many research groups, there are several aspects of H-NS that remain controversial

or completely unknown (19). Up to now, a complete, high-resolution structure of full-length H-NS, either free or complexed with DNA, has proven elusive. Structural models for the N-terminal dimerization domain have been determined by NMR spectroscopy (11,12) and x-ray crystallography (18), showing that dimerization occurs through the formation of a coiled-coil interaction motif. However, the degree of oligomerization of H-NS in solution is unclear, because dimers, tetramers, and larger oligomers have been observed under different conditions (11,20–23). An NMR spectroscopy study on the DNA-binding domain revealed that a specific sequence in the domain binds to the minor groove (13). A genome-wide analysis identified a strong correlation between H-NS binding sites and AT-rich regions on the DNA (24), and in addition, a 10-basepair (bp) high-affinity H-NS binding site was also discovered in the *proV* promoter (25). Still, the specific mechanisms for recognition of these regions by H-NS remain unclear. Furthermore, the mechanism by which an H-NS dimer determines to bind in *trans* or in *cis* mode is unknown. By probing H-NS/DNA interactions through equilibrium H-NS-mediated DNA looping scanning-force microscopy imaging and dynamic optical trap-driven unzipping assays, Wiggins et al. (15) suggested that observed DNA loops may result from the antagonistic effects of *trans*- and *cis*-binding.

Molecular simulations can complement experiments by providing details at high spatial and temporal resolution. For example, coarse-grained Monte Carlo simulations recently indicated that H-NS bridge formation occurs preferentially at planar bends in the DNA (26). In this article, we aim to shed additional light on the H-NS mediated compaction of DNA by using a Hamiltonian coarse-grained model for H-NS binding to DNA. Such models have proven

Submitted December 14, 2012, and accepted for publication February 12, 2013.

*Correspondence: marc.joyeux@ujf-grenoble.fr or j.vreede@uva.nl

Editor: Michael Feig.

© 2013 by the Biophysical Society
0006-3495/13/04/1615/8 \$2.00



to be very helpful in understanding facilitated diffusion, i.e., the various mechanisms by which proteins scan DNA sequences while searching for their target site (27–29). In this model, *trans*- and *cis*-binding are not introduced a priori, but follow instead from the explicit interaction energy function between DNA and the proteins. The results presented in this article highlight the fact that DNA compaction is indeed driven by the subtle equilibrium between several competing factors, including the deformation dynamics of the plasmid and the several binding modes of protein dimers to DNA. Moreover, simulations of DNA constrained to a planar system suggest that the conformations of DNA/H-NS complexes deposited on mica surfaces may differ substantially from those that prevail in living cells.

METHODS

Construction of the coarse-grained model was aimed at mimicking the DNA/H-NS incubation conditions used by Dame et al. (7). The [Supporting Material](#) gives a detailed description of the model. In brief, it consists of a pUC19 plasmid and 224 H-NS dimers (i.e., 1 dimer:12 bp, as in Dame et al. (7)) at a temperature of $T = 298$ K ($1 k_B T \approx 2.48$ kJ/mol) enclosed in a sphere of radius $R_0 = 0.434$ μm or a half-sphere of radius $R_0 = 0.547$ μm . As in previous work (27–30), DNA is modeled as a chain of beads, where each bead represents 15 DNA basepairs (bp). This level of coarse-graining is reasonable, because studies have shown that an H-NS DNA-binding domain occupies ~ 15 bp (31). As a consequence, the 2686-bp pUC19 plasmid is modeled as a cyclic chain of 179 beads. To keep the same level of coarse-graining, H-NS dimers are modeled as chains of three beads. The chosen equilibrium distance between two successive beads ($L_0 = 7.0$ nm) corresponds to the two N-terminal domains of H-NS dimers being arranged in anti-parallel (12) rather than in parallel (11) geometries. Electric charges are placed at the center of each bead ($-12 \bar{e}$ on DNA beads, $4 \bar{e}$ on H-NS terminal beads, and $-8 \bar{e}$ on H-NS central beads, where \bar{e} denotes the absolute charge of the electron) and the DNA molecule and the H-NS dimers interact through the sum of electrostatic terms (Debye-Hückel potentials) and excluded volume terms. The parameter χ of the excluded volume terms was chosen such that the computed enthalpy change upon a single H-NS molecule binding to DNA matches the experimental value at $T = 298$ K (31). For a dimer binding to DNA, the computed enthalpy change is $\Delta H = 11.1 k_B T$ (see [Fig. S1](#) in the [Supporting Material](#)), and the enthalpy change of an H-NS dimer binding two DNA sites in the *trans* configuration is twice this value, $22.2 k_B T$. Because at equilibrium H-NS dimers are assumed to be linear, the enthalpy change of an H-NS dimer binding two DNA sites in the *cis* mode depends on its bending rigidity G . We performed simulations with two different values of G , namely $G = 2 k_B T$ and $G = 4 k_B T$, which correspond to *cis*-binding enthalpy changes of $19.2 k_B T$ (see [Fig. S2](#)) and $16.8 k_B T$ (see [Fig. S3](#)), respectively.

The dynamics of the system was investigated by numerically integrating the Langevin equations of motion for 10 ms with a time step of 20 ps. Two different sets of simulations were performed. The first set of simulations, hereafter labeled 3D, aimed at mimicking the motion of the system in bulk buffer by allowing all molecules to move freely inside the sphere. The second set of simulations, hereafter labeled 2D, aimed at mimicking DNA molecules deposited on cleaved mica surfaces by restricting the motion of H-NS dimers to a half-sphere, and constraining the plasmid to remain in the neighborhood of the limiting disk. Four 2D simulations were run for each value of G starting from circular plasmid conformations and eight 3D simulations were run for each value of G starting from thermalized plasmid conformations. Analysis of the simulations consisted in counting every 10 μs the number of bound H-NS dimers. An H-NS dimer

was considered bound to DNA if at least one bead was within a distance of 2 nm from a DNA bead (see the [Supporting Material](#) and [Fig. S4](#) for a discussion on the choice of 2 nm for the distance threshold). Also, the nature of the bound H-NS dimers was tracked. A dimer was considered to be bound in *cis* if the two terminal beads were interacting with DNA beads separated by at most two DNA beads. If instead, the H-NS dimer was interacting with two DNA beads separated by (strictly) more than two DNA beads, the H-NS/DNA interaction was counted as a *trans* bond. Finally, the dimer was considered to be dangling, if only one bead of the dimer was interacting with the DNA. Furthermore, the radius of gyration of the plasmid, i.e., the square-root of the trace of its gyration tensor, was also computed every 10 μs .

RESULTS AND DISCUSSION

As described in Methods, the model consists of a cyclic DNA molecule with 179 binding sites and 224 H-NS dimers, which move under the action of thermal noise and interaction forces, enclosed in a sphere. When an H-NS dimer comes close to a free DNA site, binding can occur between this DNA bead and a terminal bead in the H-NS dimer, due to the electrostatic attraction between the positive charge placed on the H-NS terminal beads and the negative charge placed on the DNA bead. Subsequently, the other, dangling bead of the H-NS dimer can bind to another site on the DNA. If the second site is within three beads of the first one, the H-NS dimer has bound in *cis* mode. Alternatively, the second binding site can be located far away from the first site from a sequence point of view, resulting in an H-NS dimer bound in *trans*. All bonds between H-NS and DNA are reversible, which means that a twice-bound H-NS dimer can return to the dangling configuration and that a dangling H-NS can detach from DNA or slide along the sequence. As only *trans*-binding dimers contribute to DNA compaction (*cis*-binding and dangling dimers contribute to DNA stiffening (16)), the number of *trans*-binding H-NS dimers is the key quantity to measure DNA compaction. In contrast, *cis*-binding dimers tend to render the DNA inactive, as they prevent binding sites from participating in DNA compaction. The dangling dimers have a more versatile role. Even though they do not contribute to compaction at the current timestep, their probability to form a *trans*-binding dimer at later time-steps may be high.

The motion of DNA plays a significant role in the global dynamics of H-NS dimers in the presence of DNA. The simulations show that thermal noise, introduced by the Langevin equations of motion, is sufficient to severely deform the cyclic plasmid chain, allowing for two sites, widely separated in sequence, to eventually come close in space. Upon two sequentially distant sites approaching each other, one of three events may occur:

1. If no H-NS dimer is bound, the sites will again move apart after a short while.
2. If both sites contain a *cis*-binding or dangling H-NS dimer, both sites will also move apart again.

3. In the case of one free site and one site occupied by a dangling H-NS dimer approaching each other, *trans*-binding can occur.

A single *trans*-binding bridge is not very strong by itself and is likely to be broken by further deformation of the plasmid chain due to thermal noise. Nevertheless, a single *trans*-bound dimer keeps the two sites in close vicinity for a substantially longer time. As a consequence, additional *trans*-binding bridges are more likely to form at sites close to the first *trans*-binding dimer, provided that other pairs of free and dangling dimer sites are available. Therefore, under suitable conditions (7) the first *trans*-binding dimer can act as a seed to propagate compaction, a mechanism sometimes referred to as cooperativity.

The effect of the H-NS dimer *cis*-binding energy on DNA compaction

Because there are many interacting possibilities at each step, the final state of the system will be very sensitive to small changes in the description of the interactions. To begin, we investigated the effect of changing the *cis* interaction energy. This energy depends on the bending rigidity G . At higher values of G , the H-NS dimer is stiffer and less likely to bend. Therefore, we expect that at higher values of G , fewer H-NS dimers will bind in *cis* mode, because bending of the H-NS molecule is required for *cis*-binding. We performed three-dimensional simulations for $G = 2 k_B T$ and $G = 4 k_B T$, which correspond to *cis*-binding enthalpy differences ΔH of $19.2 k_B T$ and $16.8 k_B T$, respectively. Fig. 1 shows the time evolution of the number of H-NS dimers bound to DNA for $G = 2 k_B T$ (bottom plot) and $G = 4 k_B T$ (top plot), partitioned in dangling dimers, *cis*- and *trans*-binding dimers. For both values of G , the average number of dangling proteins is comparable, tending toward a value close to 50 at long times. In contrast, there is a huge difference in the number of *cis*-binding dimers. Indeed, for $G = 2 k_B T$ the average number of *cis*-binding dimers tends toward 25 or 30 at long times, while this number remains very small, close to 5, for $G = 4 k_B T$. Conversely, the number of *trans*-binding dimers at long times is close to 5 and 25 for $G = 2 k_B T$ and $G = 4 k_B T$, respectively. This indicates that the moderate difference in the value of the *cis*-binding energy is sufficient to induce large changes in the average number of *cis*- and *trans*-binding dimers. In contrast, the time evolution of the fraction of DNA sites occupied by H-NS dimers, shown in Fig. S5, indicates that the value of G has little effect on the occupation of DNA sites by H-NS. Indeed, the fraction of occupied sites after 10 ms is close to 0.65 for both values of G .

The huge difference in the number of *cis*- and *trans*-binding dimers for the two different bending rigidities has profound effects on the dynamics of the condensed plasmid, as illustrated in Fig. 2. This figure shows the occupation of

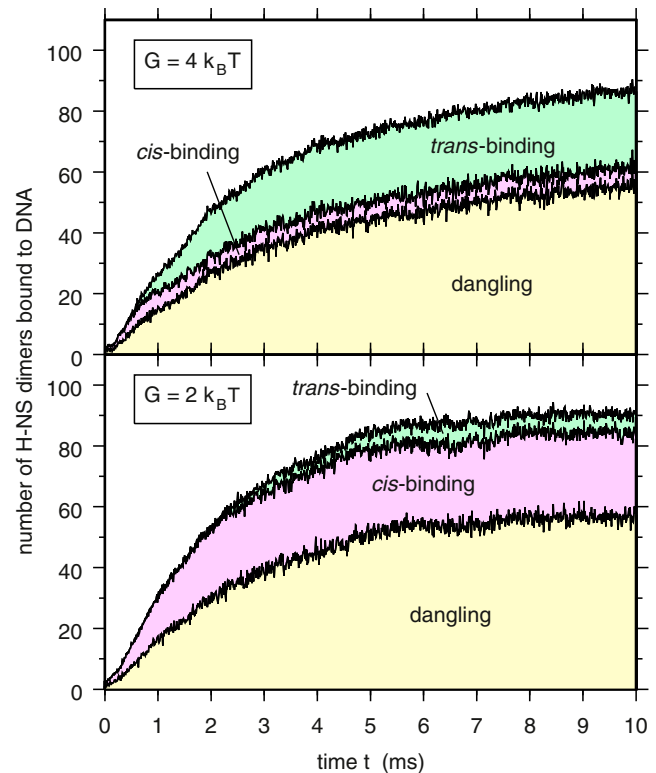


FIGURE 1 Time evolution of the number of H-NS dimers bound to DNA (3D simulations). Area charts showing the time evolution of the number of H-NS dimers bound to DNA, and the partitioning into dangling dimers and *cis*- and *trans*-binding dimers, for 3D simulations with $G = 2 k_B T$ (bottom plot) and $G = 4 k_B T$ (top plot). The system consists of 224 H-NS dimers and one plasmid with 179 binding sites. Results were averaged over eight different trajectories starting from thermalized plasmid conformations.

DNA sites by *trans*-binding H-NS dimers, which contribute to compaction, for $G = 2 k_B T$ (bottom plot) and $G = 4 k_B T$ (top plot). At $G = 4 k_B T$, the large number of *trans*-binding dimers facilitates many bridges between DNA sites located everywhere in the sequence. As a result, the plasmid molecule acquires a globular shape, which changes little with time, as demonstrated by the almost constant value of its radius of gyration, plotted in Fig. 3 for a single simulation and in the top plot of Fig. S6 for eight different simulations. In contrast, for $G = 2 k_B T$, the small number of *trans*-binding H-NS dimers allows for only a few, short-lived bridges, which form and break with fluctuations in the plasmid conformation (see Fig. 2). As a consequence, the plasmid molecule displays a very rich dynamics, with compact shapes following more loosely packed conformations and vice versa. This behavior is again clearly reflected in the time evolution of the radius of gyration of the plasmid, shown in Fig. 3 for a single simulation and in the bottom plot of Fig. S6 for eight different simulations. Movie S1 and Movie S2 in the Supporting Material, showing the time evolution of the plasmid conformations for the simulations also shown in Figs. 2 and 3, clearly illustrate the differences in the plasmid dynamics.

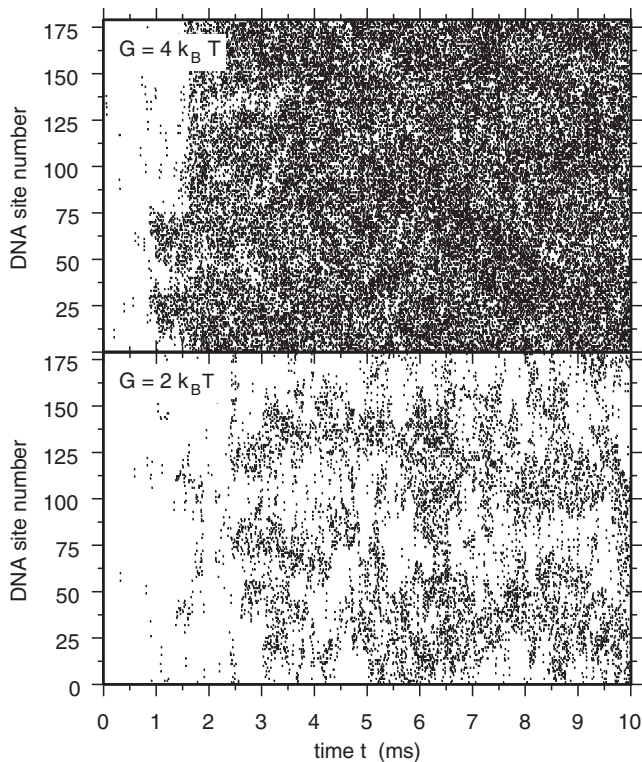


FIGURE 2 Time evolution of bridged DNA sites (3D simulations). Diagrams showing the time evolution of bridged DNA sites for single 3D simulations with $G = 2 k_B T$ (bottom plot) and $G = 4 k_B T$ (top plot). DNA sites are numbered from 1 to 179 and reported on the vertical axis. Every $10 \mu s$, the DNA sites occupied by a *trans*-binding H-NS dimer are listed and ticks are placed in the diagram at the corresponding locations.

A comparison of H-NS mediated compaction in bulk and on a surface

The simulations discussed above mimicked bulk solution conditions. However, in the scanning force microscopy imaging experiments of Dame et al. (7), solutions containing DNA/H-NS complexes were deposited on freshly cleaved mica surfaces followed by gentle drying of the mica disks. Deposition on a surface plate may significantly alter the conformations displayed by naked DNA in comparison to the bulk solution situation (32). Magnesium ions mediate the binding of DNA to mica, by forming bridges between the negative charges on the phosphate backbone and the negatively charged mica sites. These bridges are strong, because DNA molecules do not return into the solution after deposition onto the surface under standard conditions (32). Moreover, when deposited on untreated freshly cleaved mica, DNA molecules equilibrate onto the surface as in an ideal 2D solution, while the conformations of DNA molecules deposited on glow-discharged or H^+ -exchanged mica resemble the projection of the bulk 3D conformations onto a 2D plane (32). The latter results from increasing the interaction energy between DNA and the surface by discharging, soaking, or rinsing the mica

plate with deionized water, which displaces the metal ions. These stronger binding energies prevent lateral diffusion and equilibration of the DNA molecule.

To our knowledge, the deposition of DNA/H-NS complexes on mica surfaces has not been studied in such detail. It is, however, interesting to note that Dame et al. (7) deposited the complexes on freshly cleaved surfaces without prior treatment, representing conditions where naked DNA would equilibrate as in an ideal 2D solution. We therefore investigated the effects of constraining the DNA plasmid to remain close to a plane (see [Methods](#) and the [Supporting Material](#) for more detail on these calculations). Constraining DNA to move in 2D rather than in 3D has a huge impact on the elastic bending energy, the apparent rigidity of the molecule, the number of *cis*- and *trans*-bonds that can be formed, and therefore on the whole compaction dynamics. Fig. 4 shows the time evolution of the number of H-NS dimers bound to DNA obtained from 2D simulations with $G = 2 k_B T$ (bottom plot) and $G = 4 k_B T$ (top plot), including the partitioning in dangling dimers and *cis*- and *trans*-binding dimers. Comparison of 2D and 3D simulations indicates that the general trends observed in 3D are preserved in 2D, in particular the swapping of the numbers of *cis*- and *trans*-binding H-NS dimers when switching from $G = 4 k_B T$ to $G = 2 k_B T$. However, the number of *trans*-binding dimers is substantially smaller in 2D than in 3D for both values of G . For $G = 2 k_B T$, this number has become so small that it cannot be distinguished anymore in the bottom plot of Fig. 4. When looking at the degree of compaction, measured by the number of DNA sites occupied by *trans*-binding H-NS dimers, it is clear that compaction hardly takes place in 2D for $G = 2 k_B T$ (bottom plot of Fig. 5), while it is rapid and quite homogeneous for $G = 4 k_B T$ (top plot of Fig. 5).

The differences between condensed conformations in 2D and 3D are even more striking. For $G = 4 k_B T$, condensed planar plasmid molecules resemble coil-shaped filaments, caused by the many parallel *trans*-binding H-NS dimers (see Fig. 6), whereas in 3D they adopt a more globular shape (see the *snapshots* in Fig. 3 and see [Movie S1](#)). Similarly, for $G = 2 k_B T$ the (eventually) condensed planar plasmids consist of open loops connected by bridges (see Fig. 6), which differ markedly from the more intricate conformations observed in 3D (see the *snapshots* in Fig. 3 and see [Movie S2](#)). Interestingly, the condensed conformations computed in 2D for $G = 2 k_B T$ are quite similar to those observed by Dame et al., who reported that open end-loops are present on all observed DNA/H-NS complexes (7). It is therefore tempting to conclude that the correct value for G , i.e., the one that correctly predicts the experimental compaction results, is $G = 2 k_B T$. However, this conclusion is premature because the reproducible observation of open end-loops may merely reflect the higher affinity of the mica surface for complexes

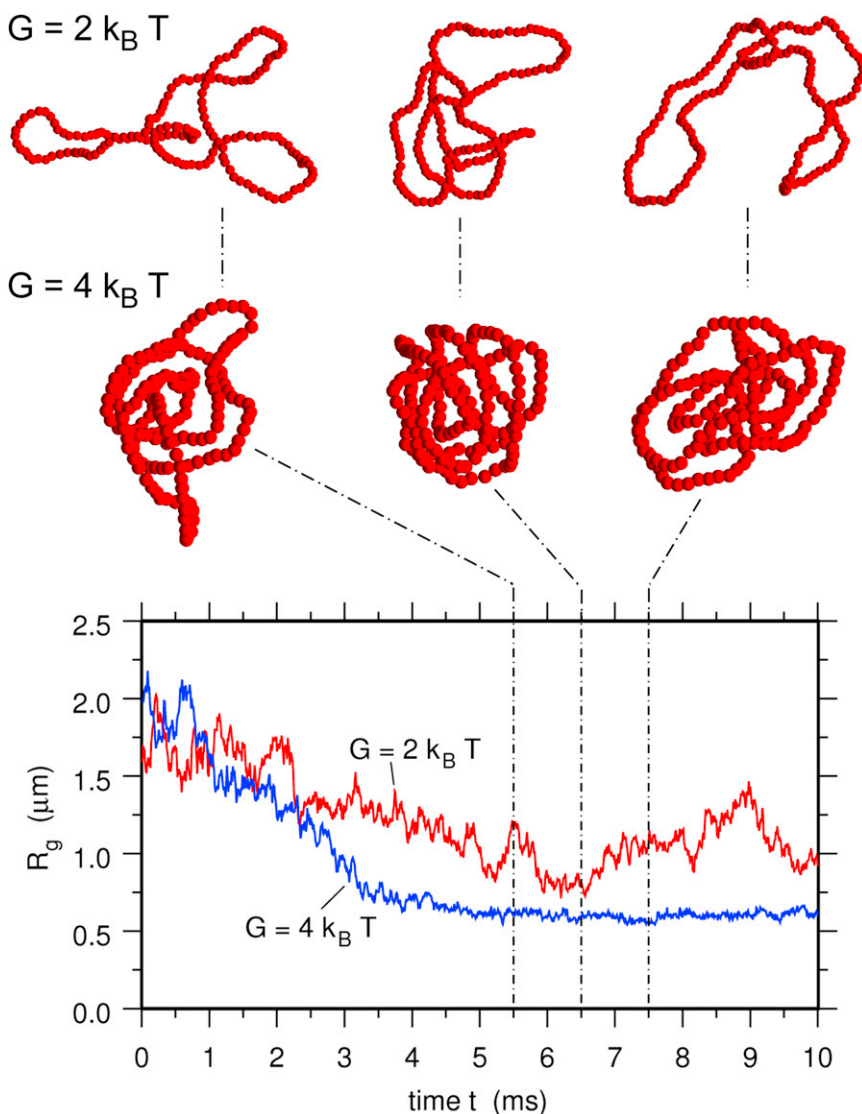


FIGURE 3 Time evolution of the radius of gyration of the plasmid molecule (3D simulations). (Bottom plot) Time evolution of the radius of gyration of the plasmid molecule for single simulations with $G = 2 k_B T$ and $G = 4 k_B T$. (Insets above plot) Conformations of the plasmid molecule at $t = 5.5$ ms, 6.5 ms, and 7.5 ms for $G = 2 k_B T$ (top row) and $G = 4 k_B T$ (second row). H-NS dimers are not shown for clarity.

with open DNA end-loops than for completely condensed DNA molecules (7). Stated in other words, if coil-shaped filaments detach preferentially from the surface during rinsing, then one would observe only complexes with open end-loops during scanning force microscopy experiments, even if coil-shaped filaments had also formed during the equilibration phase. Simulations with a more realistic description of the interactions between DNA and the surface, thus facilitating a comparison between the surface binding strengths of coiled versus open end-looped conformations, would therefore be of great interest in obtaining a firm estimate for the value of G .

Nevertheless, the results of the 2D simulations agree much better with experimentally observed condensed complexes than those of the 3D simulations. This suggests that relaxation of the DNA/H-NS complexes on a mica surface strongly affects their geometry and that the conformations observed in the course of AFM experiments may consequently not be the mere projections of bulk

conformations on the surface, but may instead differ significantly from those that prevail in living cells.

CONCLUSION

In this work, we have constructed a coarse-grained model description of the compaction of bacterial DNA by H-NS proteins. The level of coarse-graining of the model is sufficiently high to allow for the numerical integration of trajectories for 10 ms but fine enough to match the experimental observation that each bound H-NS molecule occupies ~ 15 bp. Results of the simulations highlight the fact that DNA compaction is driven by the subtle equilibrium among several competing factors, including the deformation dynamics of the plasmid and the several binding modes of protein dimers, i.e., dangling configuration and *cis*- and *trans*-binding. In particular, the simulations showed that condensed DNA conformations are very sensitive to the binding energy difference between the *cis*- and

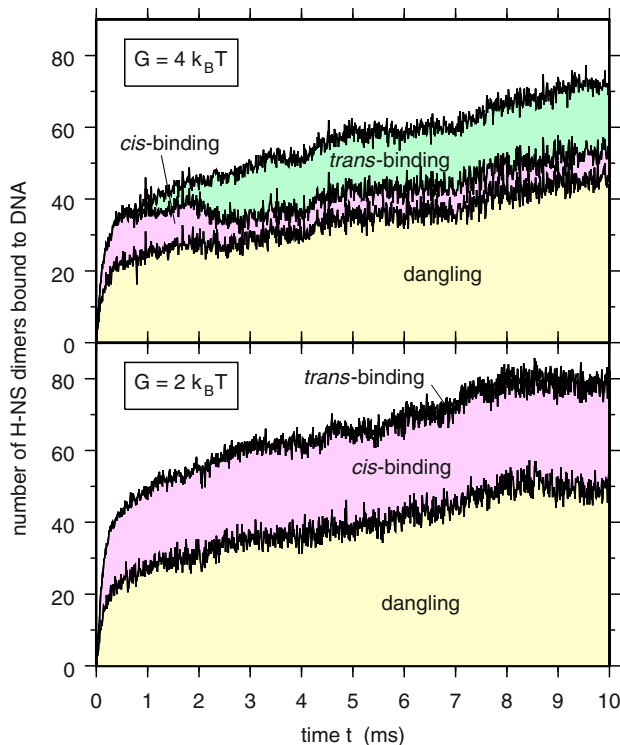


FIGURE 4 Time evolution of the number of H-NS dimers bound to DNA (2D simulations). Area charts showing the time evolution of the number of H-NS dimers bound to DNA, and the partitioning into dangling dimers and *cis*- and *trans*-binding dimers, for 2D simulations with $G = 2 k_B T$ (bottom plot) and $G = 4 k_B T$ (top plot). The system consists of 224 H-NS dimers and one plasmid with 179 binding sites. Results were averaged over four different trajectories starting from circular plasmid conformations.

trans-binding conformations. If H-NS *cis*-binding dimers are not substantially less stable than *trans*-binding dimers, then *cis*-binding and dangling dimers occupy most of DNA binding sites, and the number of *trans*-binding dimers, equal to the number of bridges between two DNA sites that are at least three beads apart, remains small. This leads to moderately condensed DNA conformations, which are still able to deform strongly. In contrast, if *cis*-binding dimers are substantially less stable than the *trans*-binding ones, then the number of *trans*-binding proteins becomes large, resulting in DNA rapidly acquiring a globular conformation, which changes little in time. Our simulations also pointed out that the conformations of DNA/H-NS complexes are significantly different in 2D and in 3D. This observation suggests that the relaxation of complexes on a mica surface has a strong influence on the observed conformations and, consequently, that conformations observed on mica plates may differ from those that prevail in living cells.

There are several lines along which the model described in this work can be extended and improved.

First of all, a more realistic description of the interactions between the plasmid and the mica surface would be of great interest to confirm that the conformations observed during scanning force microscopy experiments indeed result from

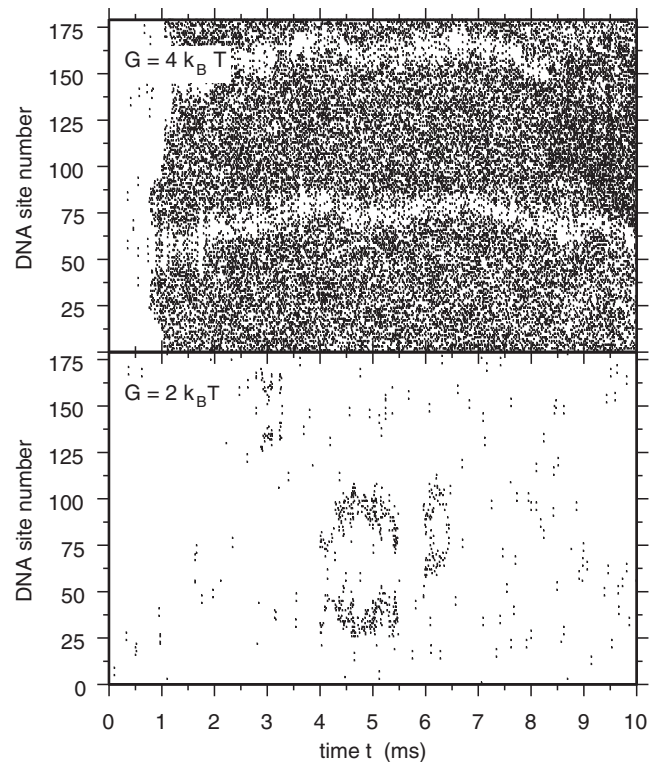


FIGURE 5 Time evolution of bridged DNA sites (2D simulations). Diagrams showing the time evolution of bridged DNA sites for single 2D simulations with $G = 2 k_B T$ (bottom plot) and $G = 4 k_B T$ (top plot). DNA sites are numbered from 1 to 179 and reported on the vertical axis. Every $10 \mu s$, the DNA sites occupied by a *trans*-binding H-NS dimer are listed and ticks are placed in the diagram at the corresponding locations.

the equilibration of globular bulk conformations on the mica surface. To this end, one should first construct a suitable interaction term between DNA and the surface, which would lead to correct predictions for the dynamics of naked

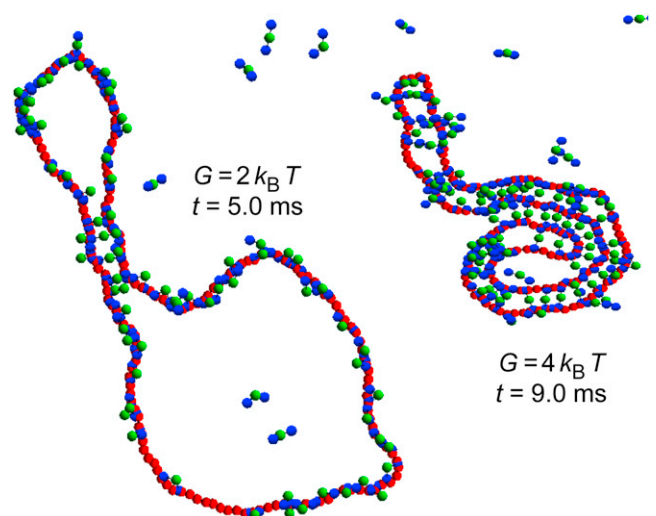


FIGURE 6 Typical 2D plasmid conformations. Typical conformations of the plasmid for the trajectories shown in Fig. 5. Snapshots were taken at $t = 5.0$ ms (for $G = 2 k_B T$) and $t = 9.0$ ms (for $G = 4 k_B T$), respectively.

DNA deposition, in particular regarding the complete relaxation of DNA at low surface charge density and the freezing of lateral motion at higher charge density. By using this interaction potential for DNA/H-NS complexes, the simulations can shed light on whether H-NS bridges are sufficient to prevent equilibration or if the bridges that exist before deposition break and/or reorganize during deposition and equilibration.

A straightforward extension of this work consists of performing similar simulations close to in vivo conditions, instead of the experimental conditions of Dame et al. (7). As a necessary benchmark to adjust the parameters of the model, the simulations reported in this article were indeed performed with one 2686 bp plasmid and 224 H-NS dimers to allow for comparison with experiments. In contrast, bacterial DNA may be several million basepairs long and each cell contains approximately one H-NS dimer per 200 DNA basepairs, instead of one H-NS dimer per 12 DNA basepairs as in the experiment by Dame et al. (7). Performing simulations in in vivo conditions could provide interesting information, such as, for example, an estimation of the compaction factor due to H-NS, but will also certainly be very expensive from the computational point of view.

Yet another step closer to simulating the actual bacterial genome would involve including additional different proteins, known to play an important role in the compaction of bacterial DNA, such as HU, IHF, StpA, Dps, or FIS. StpA, which is homologous to H-NS, is also able to form bridges between two separate DNA duplexes (33). During the stationary phase, Dps binds to chromosomal DNA, thereby forming a stable complex called a biocrystal, but the mode of the DNA/Dps interaction is not yet fully understood (34). Fis induces compaction of DNA essentially due to bending (35). At last, HU and IHF, which are homologous to each other, condense DNA by bending and undertwisting it (36). Introducing all these different proteins into a single model is a formidable task, but one could, as a first step, investigate the essential properties of each of them by using a similar mesoscopic model as used here for H-NS.

SUPPORTING MATERIAL

Model and Simulations section, two movies, six figures, and references (37–40) are available at [http://www.biophysj.org/biophysj/supplemental/S0006-3495\(13\)00262-2](http://www.biophysj.org/biophysj/supplemental/S0006-3495(13)00262-2).

REFERENCES

- Johnson, R. C., L. M. Johnson, ..., J. F. Gardner. 2005. Major nucleoid proteins in the structure and function of the *Escherichia coli* chromosome. In *The Bacterial Chromosome*. N. P. Higgins, editor. American Society for Microbiology, Washington, DC. 65–132.
- Dame, R. T. 2005. The role of nucleoid-associated proteins in the organization and compaction of bacterial chromatin. *Mol. Microbiol.* 56:858–870.
- Luijsterburg, M. S., M. F. White, ..., R. T. Dame. 2008. The major architects of chromatin: architectural proteins in bacteria, archaea and eukaryotes. *Crit. Rev. Biochem. Mol. Biol.* 43:393–418.
- Wang, W., G.-W. Li, ..., X. Zhuang. 2011. Chromosome organization by a nucleoid-associated protein in live bacteria. *Science*. 333:1445–1449.
- Browning, D. F., D. C. Grainger, and S. J. W. Busby. 2010. Effects of nucleoid-associated proteins on bacterial chromosome structure and gene expression. *Curr. Opin. Microbiol.* 13:773–780.
- Dillon, S. C., A. D. S. Cameron, ..., C. J. Dorman. 2010. Genome-wide analysis of the H-NS and Sfh regulatory networks in *Salmonella typhimurium* identifies a plasmid-encoded transcription silencing mechanism. *Mol. Microbiol.* 76:1250–1265.
- Dame, R. T., C. Wyman, and N. Goosen. 2000. H-NS mediated compaction of DNA visualized by atomic force microscopy. *Nucleic Acids Res.* 28:3504–3510.
- Dame, R. T., M. C. Noom, and G. J. L. Wuite. 2006. Bacterial chromatin organization by H-NS protein unraveled using dual DNA manipulation. *Nature*. 444:387–390.
- White-Ziegler, C. A., and T. R. Davis. 2009. Genome-wide identification of H-NS-controlled, temperature-regulated genes in *Escherichia coli* K-12. *J. Bacteriol.* 191:1106–1110.
- Hommais, F., E. Krin, ..., P. Bertin. 2001. Large-scale monitoring of pleiotropic regulation of gene expression by the prokaryotic nucleoid-associated protein, H-NS. *Mol. Microbiol.* 40:20–36.
- Esposito, D., A. Petrovic, ..., J. E. Ladbury. 2002. H-NS oligomerization domain structure reveals the mechanism for high order self-association of the intact protein. *J. Mol. Biol.* 324:841–850.
- Bloch, V., Y. Yang, ..., M. Kochoyan. 2003. The H-NS dimerization domain defines a new fold contributing to DNA recognition. *Nat. Struct. Biol.* 10:212–218.
- Gordon, B. R. G., Y. Li, ..., J. Liu. 2011. Structural basis for recognition of AT-rich DNA by unrelated xenogeneic silencing proteins. *Proc. Natl. Acad. Sci. USA*. 108:10690–10695.
- Dorman, C. J., J. C. D. Hinton, and A. Free. 1999. Domain organization and oligomerization among H-NS-like nucleoid-associated proteins in bacteria. *Trends Microbiol.* 7:124–128.
- Wiggins, P. A., R. T. Dame, ..., G. J. Wuite. 2009. Protein-mediated molecular bridging: a key mechanism in biopolymer organization. *Biophys. J.* 97:1997–2003.
- Liu, Y. J., H. Chen, ..., J. Yan. 2010. A divalent switch drives H-NS/DNA-binding conformations between stiffening and bridging modes. *Genes Dev.* 24:339–344.
- Navarre, W. W., S. Porwollik, ..., F. C. Fang. 2006. Selective silencing of foreign DNA with low GC content by the H-NS protein in *Salmonella*. *Science*. 313:236–238.
- Arold, S. T., P. G. Leonard, ..., J. E. Ladbury. 2010. H-NS forms a superhelical protein scaffold for DNA condensation. *Proc. Natl. Acad. Sci. USA*. 107:15728–15732.
- Navarre, W. W. 2010. H-NS as a defense system. In *Bacterial Chromatin*. R. T. Dame and C. J. Dorman, editors. Springer, New York. 251–322.
- Falconi, M., B. Colonna, ..., C. O. Gualerzi. 1998. Thermoregulation of *Shigella* and *Escherichia coli* EIEC pathogenicity. A temperature-dependent structural transition of DNA modulates accessibility of *virF* promoter to transcriptional repressor H-NS. *EMBO J.* 17:7033–7043.
- Ueguchi, C., T. Suzuki, ..., T. Mizuno. 1996. Systematic mutational analysis revealing the functional domain organization of *Escherichia coli* nucleoid protein H-NS. *J. Mol. Biol.* 263:149–162.
- Clare, P. S., T. Lundbäck, ..., J. E. Ladbury. 2002. Oligomerization of the chromatin-structuring protein H-NS. *Mol. Microbiol.* 36:962–972.
- Ceschini, S., G. Lupidi, ..., M. Angeletti. 2000. Multimeric self-assembly equilibria involving the histone-like protein H-NS. A thermodynamic study. *J. Biol. Chem.* 275:729–734.

24. Lucchini, S., G. Rowley, ..., J. C. Hinton. 2006. H-NS mediates the silencing of laterally acquired genes in bacteria. *PLoS Pathog.* 2:e81.
25. Bouffartigues, E., M. Buckle, ..., S. Rimsky. 2007. H-NS cooperative binding to high-affinity sites in a regulatory element results in transcriptional silencing. *Nat. Struct. Mol. Biol.* 14:441–448.
26. de Vries, R. 2011. Influence of mobile DNA-protein-DNA bridges on DNA configurations: coarse-grained Monte-Carlo simulations. *J. Chem. Phys.* 135:125104.
27. Florescu, A.-M., and M. Joyeux. 2009. Description of nonspecific DNA-protein interaction and facilitated diffusion with a dynamical model. *J. Chem. Phys.* 130:015103.
28. Florescu, A.-M., and M. Joyeux. 2009. Dynamical model of DNA protein interaction: effect of protein charge distribution and mechanical properties. *J. Chem. Phys.* 131:105102.
29. Florescu, A.-M., and M. Joyeux. 2010. Comparison of kinetic and dynamical models of DNA-protein interaction and facilitated diffusion. *J. Phys. Chem. A.* 114:9662–9672.
30. Jian, H., A. Vologodskii, and T. Schlick. 1997. A combined wormlike-chain and bead model for dynamic simulations of long linear DNA. *J. Comput. Phys.* 136:168–179.
31. Ono, S., M. D. Goldberg, ..., J. E. Ladbury. 2005. H-NS is a part of a thermally controlled mechanism for bacterial gene regulation. *Biochem. J.* 391:203–213.
32. Rivetti, C., M. Guthold, and C. Bustamante. 1996. Scanning force microscopy of DNA deposited onto mica: equilibration versus kinetic trapping studied by statistical polymer chain analysis. *J. Mol. Biol.* 264:919–932.
33. Lim, C. J., Y. R. Whang, ..., J. Yan. 2012. Gene silencing H-NS paralogue StpA forms a rigid protein filament along DNA that blocks DNA accessibility. *Nucleic Acids Res.* 40:3316–3328.
34. Saier, Jr., M. H. 2008. The bacterial chromosome. *Crit. Rev. Biochem. Mol. Biol.* 43:89–134.
35. Skoko, D., D. Yoo, ..., R. C. Johnson. 2006. Mechanism of chromosome compaction and looping by the *Escherichia coli* nucleoid protein Fis. *J. Mol. Biol.* 364:777–798.
36. Czapla, L., D. Swigon, and W. K. Olson. 2008. Effects of the nucleoid protein HU on the structure, flexibility, and ring-closure properties of DNA deduced from Monte Carlo simulations. *J. Mol. Biol.* 382: 353–370.
37. Frank-Kamenetskii, M. D., A. V. Lukashin, ..., A. V. Vologodskii. 1985. Torsional and bending rigidity of the double helix from data on small DNA rings. *J. Biomol. Struct. Dyn.* 2:1005–1012.
38. Stigter, D. 1977. Interactions of highly charged colloidal cylinders with applications to double-stranded. *Biopolymers.* 16:1435–1448.
39. Vologodskii, A. V., and N. R. Cozzarelli. 1995. Modeling of long-range electrostatic interactions in DNA. *Biopolymers.* 35:289–296.
40. Sivaramakrishnan, S., J. Sung, ..., J. A. Spudich. 2009. Combining single-molecule optical trapping and small-angle x-ray scattering measurements to compute the persistence length of a protein ER/K α -helix. *Biophys. J.* 97:2993–2999.

**A model of H-NS mediated compaction of bacterial DNA
- Supporting Material -**

Marc JOYEUX

*Laboratoire Interdisciplinaire de Physique (CNRS UMR5588),
Université Joseph Fourier Grenoble 1, BP 87, 38402 St Martin d'Hères, France*

and Jocelyne VREEDE

*Van't Hoff Institute for Molecular Sciences, University of Amsterdam,
P.O. Box 94157, 1090 GD Amsterdam, The Netherlands*

MODEL AND SIMULATIONS

The model was built to mimic the H-NS/DNA incubation conditions used in the work of Dame and co-workers (1). It consists of one pUC19 plasmid and $P=224$ H-NS dimers at a temperature $T=298$ K ($1 k_B T \approx 2.48$ kJ/mol) enclosed either in a sphere of radius $R_0 = 0.434$ μm or a half-sphere of radius $R_0 = 0.547$ μm . These values of R_0 lead to the same plasmid and H-NS concentrations as the 85 ng of DNA with 450 ng of H-NS diluted in 10 μl H-NS BB used in (1). As in previous work (2-5), DNA was modelled as a chain of beads with hydrodynamic radius $a = 1.78$ nm separated at equilibrium by a distance $l_0 = 5.0$ nm. Each bead actually represents 15 base pairs, so that the pUC19 plasmid with 2686 bp was modelled as a cyclic chain of $n=179$ beads. Each bead had an effective charge $\approx -12 \bar{e}$ placed at its centre, where \bar{e} denotes the absolute charge of the electron. This effective charge corresponds to the product of the known linear charge density of DNA ($-2.43 \bar{e}/\text{nm}$) by the equilibrium distance $l_0 = 5.0$ nm between two successive beads. Based on crystallographic data (6), each H-NS dimer was modelled as a chain of 3 beads with the same hydrodynamic radius $a = 1.78$ nm separated at equilibrium by a distance $L_0 = 7.0$ nm. An effective charge $-e_{\text{DNA}}/3 \approx 4 \bar{e}$ was placed at the centre of each terminal bead and a charge $2e_{\text{DNA}}/3 \approx -8 \bar{e}$ at the centre of each central bead. The values of these effective charges were estimated by counting the number of positively and negatively charged residues in published crystallographic structures (6).

The potential energy E_{pot} of the system was taken as the sum of 5 terms

$$E_{\text{pot}} = V_{\text{DNA}} + V_{\text{PROT}} + V_{\text{PROT/PROT}} + V_{\text{DNA/PROT}} + V_{\text{wall}}, \quad (\text{S1})$$

where V_{DNA} and V_{PROT} describe the potential energy of DNA and H-NS dimers, respectively, $V_{\text{PROT/PROT}}$ the interactions between H-NS dimers, $V_{\text{DNA/PROT}}$ the interactions between DNA and H-NS dimers, and V_{wall} the repulsive wall that maintains H-NS dimers inside the sphere.

V_{DNA} was expressed, as in previous work (2-5), as a sum of three terms

$$\begin{aligned} V_{\text{DNA}} &= E_s + E_b + E_e \\ E_s &= \frac{h}{2} \sum_{k=1}^n (l_k - l_0)^2 \\ E_b &= \frac{g}{2} \sum_{k=1}^n \theta_k^2 \\ E_e &= e_{\text{DNA}}^2 \sum_{k=1}^{n-2} \sum_{K=k+2}^n H(\|\mathbf{r}_k - \mathbf{r}_K\|), \end{aligned} \quad (\text{S2})$$

where \mathbf{r}_k denotes the position of DNA bead k , $l_k = \|\mathbf{r}_k - \mathbf{r}_{k+1}\|$ the distance between two successive beads, $\theta_k = \arccos((\mathbf{r}_k - \mathbf{r}_{k+1})(\mathbf{r}_{k+1} - \mathbf{r}_{k+2}) / (\|\mathbf{r}_k - \mathbf{r}_{k+1}\| \|\mathbf{r}_{k+1} - \mathbf{r}_{k+2}\|))$ the angle formed by three successive beads, and H is the function defined according to

$$H(r) = \frac{1}{4\pi\epsilon r} \exp\left(-\frac{r}{r_D}\right). \quad (\text{S3})$$

E_s is the bond stretching energy. In fact, this is a computational device without any biological meaning aimed at avoiding a rigid rod description. The stretching force constant was fixed at $h = 100 k_B T / l_0^2$ (see the discussion in Ref. (2) for this choice for h). E_b is the elastic bending potential. The bending rigidity constant, $g = 9.82 k_B T$, was chosen so as to provide the correct persistence length for DNA, which is 50 nm, equivalent to 10 beads (2,7). E_e is a Debye-Hückel potential, which describes repulsive electrostatic interactions between DNA beads (2,8,9). In Eq. S3, $r_D = 3.07$ nm stands for the Debye length at 0.01 M salt concentration of monovalent ions (2) and $\epsilon = 80 \epsilon_0$ for the dielectric constant of the buffer. Note that electrostatic interactions between nearest-neighbours are not included in the expression of E_e in Eq. S2, because these nearest-neighbour interactions are accounted for in the stretching and bending terms.

V_{PROT} was similarly taken as the sum of stretching and bending contributions

$$\begin{aligned}
V_{\text{PROT}} &= E_s^{(\text{P})} + E_b^{(\text{P})} \\
E_s^{(\text{P})} &= \frac{h}{2} \sum_{j=1}^P (L_{j,1} - L_0)^2 + (L_{j,2} - L_0)^2 \\
E_b^{(\text{P})} &= \frac{G}{2} \sum_{j=1}^P \Theta_j^2,
\end{aligned} \tag{S4}$$

where $L_{j,1}$, $L_{j,2}$, and Θ_j , denote the distances between the terminal beads and the central bead and the angle formed by the three beads for the j^{th} H-NS dimer. The value of the bending rigidity G was estimated by noticing that the N-terminal oligomerization domain and the C-terminal DNA-binding domain of H-NS are linked principally by a long α -helix. Since the measured persistence length ξ of α -helices is close to 15 nm (10) and is related to the bending rigidity through $G = k_{\text{B}}T\xi / L_0$, it was estimated that G is of the order of a few $k_{\text{B}}T$ for H-NS. Application of the formula leads to $G \approx 2k_{\text{B}}T$, but this value can of course only be considered as a rough estimate. As discussed in more detail below and in the main text, we actually used two different values for G in the simulations, namely $G = 2k_{\text{B}}T$ and $G = 4k_{\text{B}}T$, because these values lead to different amounts of H-NS binding in *trans* and, as a consequence, to different levels of DNA compaction.

The interaction between H-NS dimers, $V_{\text{PROT/PROT}}$, was taken as the sum of (attractive or repulsive) electrostatic terms and (repulsive) excluded volume terms, with the latter ones only contributing if the corresponding electrostatic interactions are attractive, *i.e.* between the terminal beads $m=1$ and $m=3$ of one dimer and the central bead $m=2$ of the other dimer

$$\begin{aligned}
V_{\text{PROT/PROT}} &= E_e^{(\text{P/P})} + E_{ev}^{(\text{P/P})} \\
E_e^{(\text{P/P})} &= \sum_{j=1}^P \sum_{m=1}^3 \sum_{J=j+1}^P \sum_{M=1}^3 e_{jm} e_{JM} H(\|\mathbf{R}_{jm} - \mathbf{R}_{JM}\|) \\
E_{ev}^{(\text{P/P})} &= \chi \sum_{j=1}^P \sum_{\substack{J=1 \\ J \neq j}}^P \left(\frac{e_{j1} e_{J2}}{e_{\text{DNA}}^2} \right) F(\|\mathbf{R}_{j1} - \mathbf{R}_{J2}\|) + \left(\frac{e_{j3} e_{J2}}{e_{\text{DNA}}^2} \right) F(\|\mathbf{R}_{j3} - \mathbf{R}_{J2}\|),
\end{aligned} \tag{S5}$$

where \mathbf{R}_{jm} denotes the position of bead m of protein dimer j , e_{jm} the charge placed at its centre, χ is a constant equal to $\chi = 0.15 k_{\text{B}}T$, and F is the function defined according to

$$\begin{aligned}
\text{if } r \leq 2^{3/2} a : F(r) &= 4 \left(\left(\frac{2a}{r} \right)^4 - \left(\frac{2a}{r} \right)^2 \right) + 1 \\
\text{if } r > 2^{3/2} a : F(r) &= 0 .
\end{aligned} \tag{S6}$$

It should be noted that electrostatic attractive interactions between the terminal beads of one H-NS dimer and the central bead of another H-NS dimer are too weak to allow for the

formation of long-lived bonds between these two dimers. Consequently, the model proposed here does not take oligomerization of the dimers into account. As mentioned in the Introduction section in the main text, H-NS is believed to be functional as a dimer, but trimers, tetramers and larger oligomers have been observed in solution under different conditions. If future work proves that these higher-order oligomers play an important role in H-NS mediated compaction of bacterial DNA, then the $V_{\text{PROT/PROT}}$ interaction term will have to be adapted to take oligomerization into account.

The interaction between DNA and protein dimers, $V_{\text{DNA/PROT}}$, was similarly taken as the sum of (attractive or repulsive) electrostatic terms and (repulsive) excluded volume terms, with the latter ones only contributing if the corresponding electrostatic interactions are attractive, *i.e.* between DNA beads and terminal protein beads $m=1$ and $m=3$,

$$\begin{aligned}
V_{\text{DNA/PROT}} &= E_e^{(\text{DNA/P})} + E_{ev}^{(\text{DNA/P})} \\
E_e^{(\text{DNA/P})} &= \sum_{j=1}^P \sum_{m=1}^3 \sum_{k=1}^n e_{jm} e_{\text{DNA}} H(\|\mathbf{R}_{jm} - \mathbf{r}_k\|) \\
E_{ev}^{(\text{DNA/P})} &= \chi \sum_{j=1}^P \sum_{k=1}^n \left(\frac{e_{j1}}{e_{\text{DNA}}} F(\|\mathbf{R}_{j1} - \mathbf{r}_k\|) + \frac{e_{j3}}{e_{\text{DNA}}} F(\|\mathbf{R}_{j3} - \mathbf{r}_k\|) \right).
\end{aligned} \tag{S7}$$

The confining sphere is large enough to fit the plasmid, whatever its current geometry. Indeed, the diameter of the sphere is as large as 0.868 μm for 3D simulations and 1.094 μm for 2D simulations, while the maximum length reached by the completely stretched plasmid is 0.450 μm . Since the centre of the sphere was adjusted at each time step to coincide with the centre of mass of the DNA molecule (see below), DNA beads could not exit the sphere. In order to restrain protein beads from exiting the sphere, we introduced a repulsive wall V_{wall} , which acts on the protein beads that move outside the radius of the sphere, R_0 , and repel them back into the sphere. V_{wall} was taken as a sum of repulsive terms

$$V_{\text{wall}} = 10 k_B T \sum_{j=1}^P \sum_{m=1}^3 f(\|\mathbf{R}_{jm}\|), \tag{S8}$$

where f is the function defined according to

$$\text{if } r \leq R_0 : f(r) = 0$$

$$\text{if } r > R_0 : f(r) = \left(\frac{r}{R_0} \right)^6 - 1. \tag{S9}$$

At this point, it is important to emphasize that, within this model, interactions between DNA and H-NS dimers are essentially driven by the constant χ in Eq. S7. The value

$\chi = 0.15 k_B T$ was chosen because it leads to a change in enthalpy ΔH of $11.1 k_B T$ on forming a complex between DNA and an H-NS monomer, which is comparable to experimentally determined values (11) (see Fig. S1). Moreover, the energy landscape for *cis*-binding of H-NS can be visualized by setting one H-NS terminal bead at the minimum energy location and varying the position of the other terminal bead while keeping the bond lengths at their equilibrium value L_0 . The result is shown in Fig. S2 for $G = 2 k_B T$ and in Fig. S3 for $G = 4 k_B T$. The maximum *cis*-binding enthalpy change is $19.2 k_B T$ for $G = 2 k_B T$ and $16.8 k_B T$ for $G = 4 k_B T$.

The dynamics of the system was investigated by integrating numerically the Langevin equations of motion with kinetic energy terms neglected. Practically, the updated position vector for each bead (whether DNA or protein), $\mathbf{r}^{(n+1)}$, was computed from the current position vector, $\mathbf{r}^{(n)}$, according to

$$\mathbf{r}^{(n+1)} = \mathbf{r}^{(n)} + \frac{\Delta t}{6\pi\eta a} \mathbf{F}^{(n)} + \sqrt{\frac{2 k_B T \Delta t}{6\pi\eta a}} \boldsymbol{\xi}^{(n)}, \quad (\text{S10})$$

where $\Delta t = 20$ ps is the integration time step, $\mathbf{F}^{(n)}$ the collective vector of inter-particle forces arising from the potential energy E_{pot} , $\boldsymbol{\xi}^{(n)}$ a vector of random numbers extracted at each step n from a Gaussian distribution of mean 0 and variance 1, and $\eta = 0.00089$ Pa s, the viscosity of the buffer at 298 K. After each integration step, the position of the centre of the sphere was adjusted so as to coincide with the centre of mass of the DNA molecule. Two different sets of simulations were performed. The first set of simulations, labelled 3D, aimed at mimicking the motion of the system in bulk buffer, by allowing all molecules to move freely in the sphere. The second set of simulations, labelled 2D, aimed at mimicking DNA molecules deposited on cleaved mica surfaces. To this end, the DNA molecule was constrained to remain in the neighbourhood of the $z=0$ surface, in the z -range extending from 0 to 0.5 nm, while the z -coordinate of each H-NS bead was constrained to remain positive. All simulations were run for 10 ms.

Analysis of the simulations consisted in tracking every 10 μs the number of bound H-NS dimers. It was considered that an H-NS dimer was bound to DNA if it had at least one bead within a distance of 2 nm from a DNA bead. The nature of the bound H-NS dimers was also tracked. A dimer was considered to be bound in *cis* if the two terminal beads were interacting with DNA beads separated by at most two DNA beads. If instead, the H-NS dimer was interacting with two DNA beads separated by (strictly) more than two DNA beads, the H-

NS/DNA interaction was counted as a *trans* bond. Finally, the dimer was considered to be dangling, if only one bead of the dimer was interacting with the DNA. As illustrated in Fig. S4, there is actually not much freedom in the choice of the distance threshold. Indeed, for thresholds smaller than 2.0 nm, many bound proteins are missed because of the steep repulsive wall that surrounds DNA beads (see Figs. S1-S3). On the other hand, the threshold cannot be larger than half the separation between two DNA beads, that is, 2.5 nm. The 2 nm threshold was chosen, because Fig. S4 suggests that a certain number of dangling dimers are incorrectly reassigned as *cis*-binding dimers when the threshold is increased from 2.0 to 2.5 nm. Most importantly, the estimation for the number of *trans*-binding dimers remains essentially constant in this latter range of threshold values.

The radius of gyration of the plasmid molecule, *i.e.* the square root of the trace of its gyration tensor, was also computed every 10 μ s.

The results of the simulations are discussed and illustrated in the main text. Fig. S5 additionally shows the time evolution of the occupancy ratio of DNA sites for $G = 2 k_B T$ and $G = 4 k_B T$ and Fig. S6 the time evolution of the radius of gyration of the plasmid for eight simulations with $G = 2 k_B T$ and $G = 4 k_B T$.

SUPPORTING REFERENCES

- (1) Dame, R.T., C. Wyman, and N. Goosen. 2000. H-NS mediated compaction of DNA visualised by atomic force microscopy. *Nucleic Acids Res.* 28:3504-3510.
- (2) Jian, H., A. Vologodskii, and T. Schlick. 1997. A combined wormlike-chain and bead model for dynamic simulations of long linear DNA. *J. Comp. Phys.* 136:168-179.
- (3) Florescu, A.-M., and M. Joyeux. 2009. Description of non-specific DNA-protein interaction and facilitated diffusion with a dynamical model. *J. Chem. Phys.* 130:015103.
- (4) Florescu, A.-M., and M. Joyeux. 2009. Dynamical model of DNA protein interaction: effect of protein charge distribution and mechanical properties. *J. Chem. Phys.* 131:105102.
- (5) Florescu, A.-M., and M. Joyeux. 2010. Comparison of kinetic and dynamical models of DNA-protein interaction and facilitated diffusion. *J. Phys. Chem. A* 114:9662-9672.
- (6) Arold, S.T., P.G. Leonard, G.N. Parkinson, and J.E. Ladbury. 2010. H-NS forms a superhelical protein scaffold for DNA condensation. *P. Natl. Acad. Sci. USA.* 107:15728-15732.
- (7) Frank-Kamenetskii, M.D., A.V. Lukashin, and V.V. Anshelevich. 1985. Torsional and bending rigidity of the double helix from data on small DNA rings. *J. Biomol. Struct. Dynam.* 2:1005-1012.
- (8) Stigter, D. 1977. Interactions of highly charged colloidal cylinders with applications to double-stranded DNA. *Biopolymers* 16:1435-1448.
- (9) Vologodskii, A.V., and N.R. Cozzarelli. 1995. Modeling of long-range electrostatic interactions in DNA. *Biopolymers* 35:289-296.
- (10) Sivaramakrishnan S., J. Sung, M. Ali, S. Doniach, H. Flyvbjerg, and J.A. Spudich. 2009. Combining single-molecule optical trapping and small-angle X-ray scattering measurements to compute the persistence length of a protein ER/K α -helix. *Biophys. J.* 97:2993-2999.
- (11) Ono, S., M.D. Goldberg, T. Olsson, D. Esposito, J.C.D. Hinton, and J.E. Ladbury. 2005. H-NS is a part of a thermally controlled mechanism for bacterial gene regulation. *Biochem. J.* 391:203-213.

MOVIE CAPTIONS

Movie S1 (.avi file, 4862 Ko) : **The condensed plasmid for $G=4 k_B T$.**

This movie shows the evolution of the plasmid conformations in the time interval 5.5-7.5 ms for the 3D simulation with $G = 4 k_B T$, also shown in Fig. 2 (top). The plasmid chain is shown as red beads and the H-NS dimers as green (central) and blue (terminal) beads. Frames were generated every 10 μ s.

Movie S2 (.avi file, 6129 Ko) : **The condensed plasmid for $G=2 k_B T$.**

This movie shows the evolution of the plasmid conformations in the time interval 5.5-7.5 ms for the 3D simulation with $G = 2 k_B T$ also shown in Fig. 2 (bottom). The plasmid chain is shown as red beads and the H-NS dimers as green (central) and blue (terminal) beads. Frames were generated every 10 μ s.

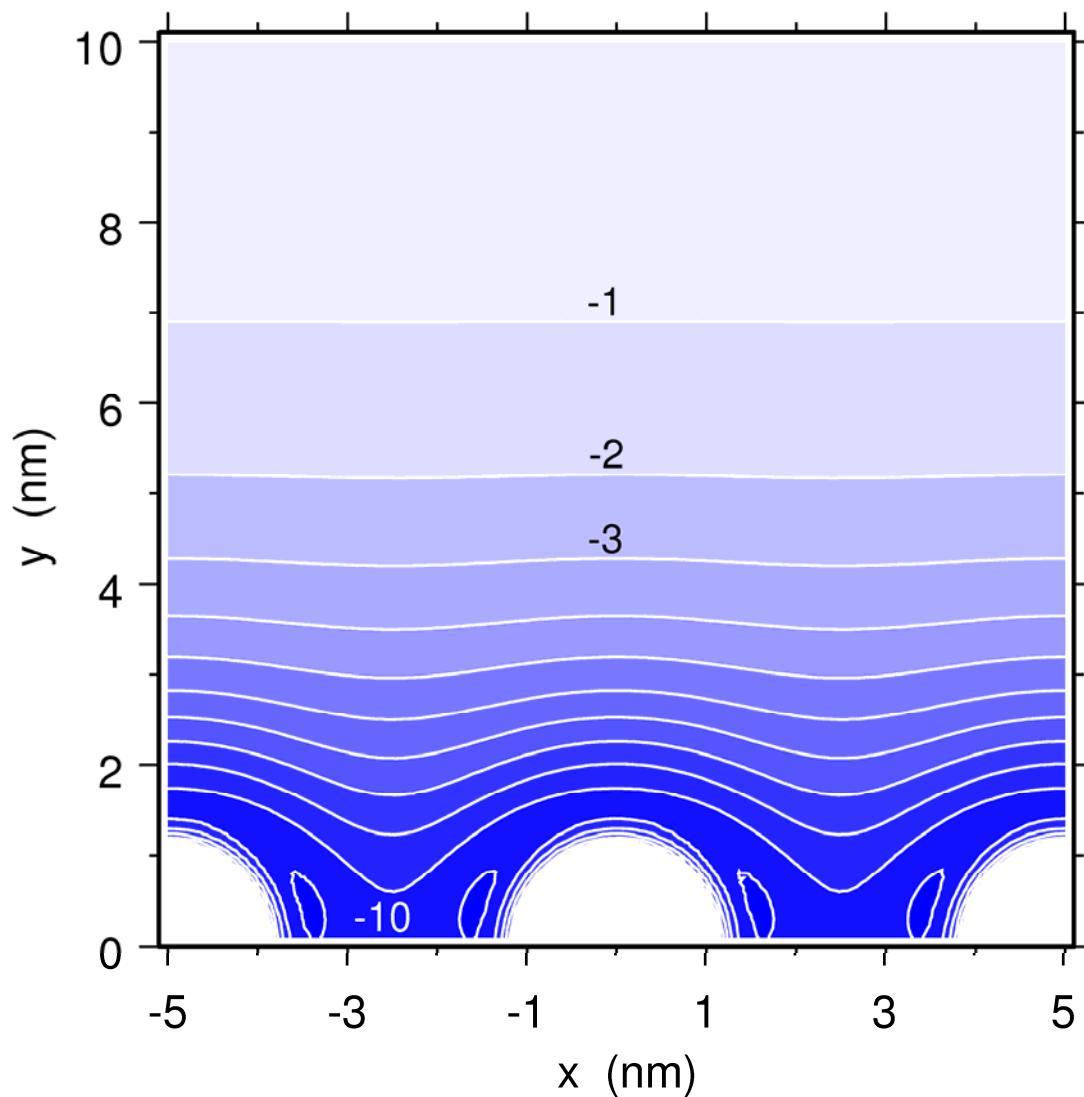


Figure S1 : Potential energy $V_{\text{DNA/PROT}}$ seen by a linear H-NS dimer oriented parallel to the y axis and with equilibrium bond lengths L_0 . (x,y) denote the coordinates of the H-NS terminal bead closest to DNA. DNA beads are located on the x axis at positions ..., -5, 0, 5, ... nm. Contours start at $-1 k_B T$ and are separated by $1 k_B T$, that is, approximately 2.48 kJ/mol at 298 K.

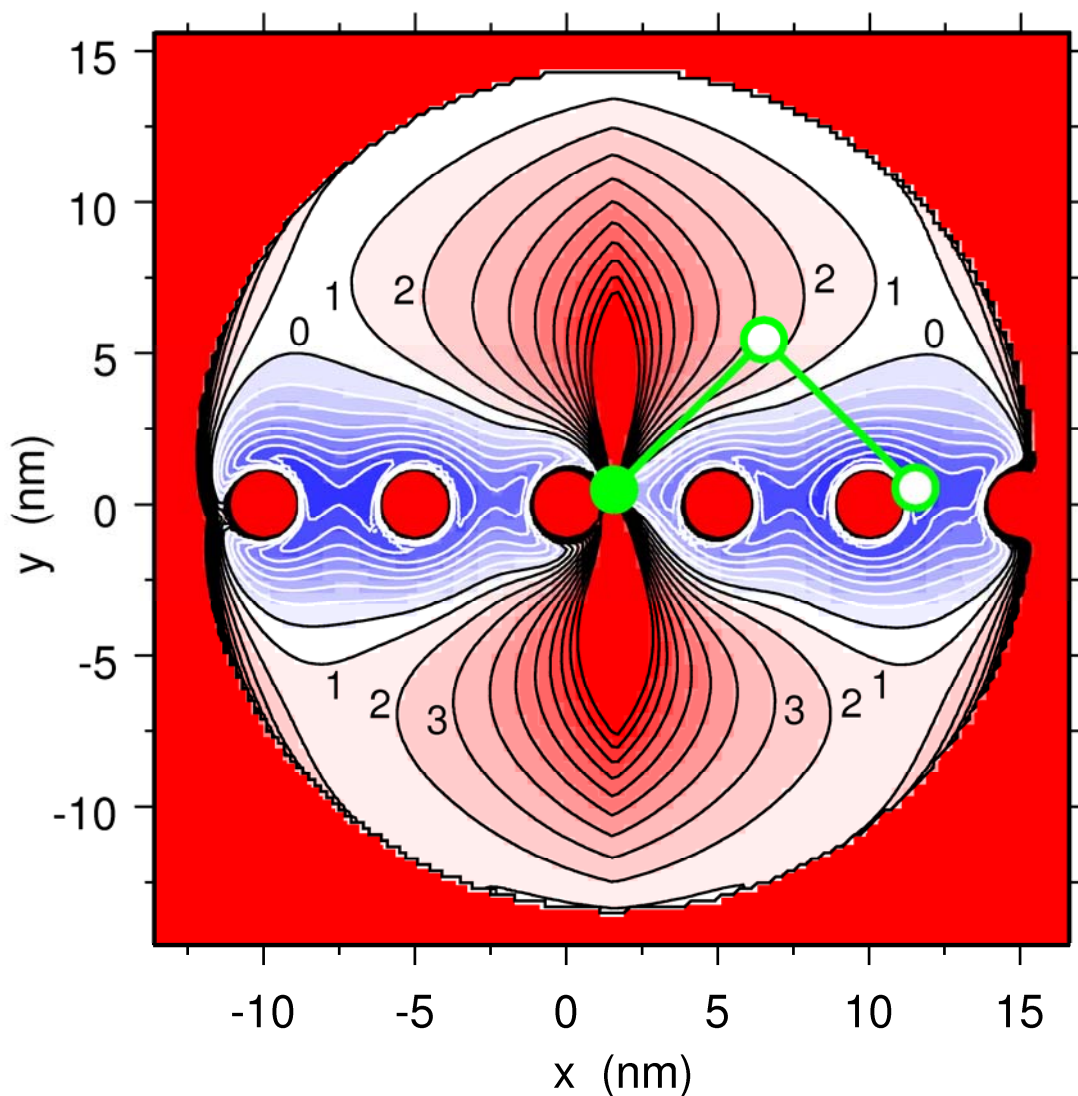


Figure S2 : Potential energy $V_{\text{DNA/PROT}}$ seen by an H-NS dimer with equilibrium bond lengths L_0 and terminal bead $m=1$ (shown as a filled green circle) sitting on the minimum energy position, for protein bending rigidity $G = 2 k_B T$. (x,y) denotes the coordinates of H-NS terminal bead $m=3$. DNA beads are located on the x axis at positions $\dots -10, -5, 0, 5, 10, 15\dots$ nm, as in Fig. S1. Energy values are plotted relative to the monomer minimum at $-11.1 k_B T$ (Fig. S1). Blue regions, with negative relative energies, therefore correspond to dimers that are more stable than the equilibrium monomer, and red regions to less stable dimers. Contours are separated by $1 k_B T$, that is, approximately 2.48 kJ/mol at 298 K. An H-NS dimer with minimum *cis*-binding energy conformation is shown in green.

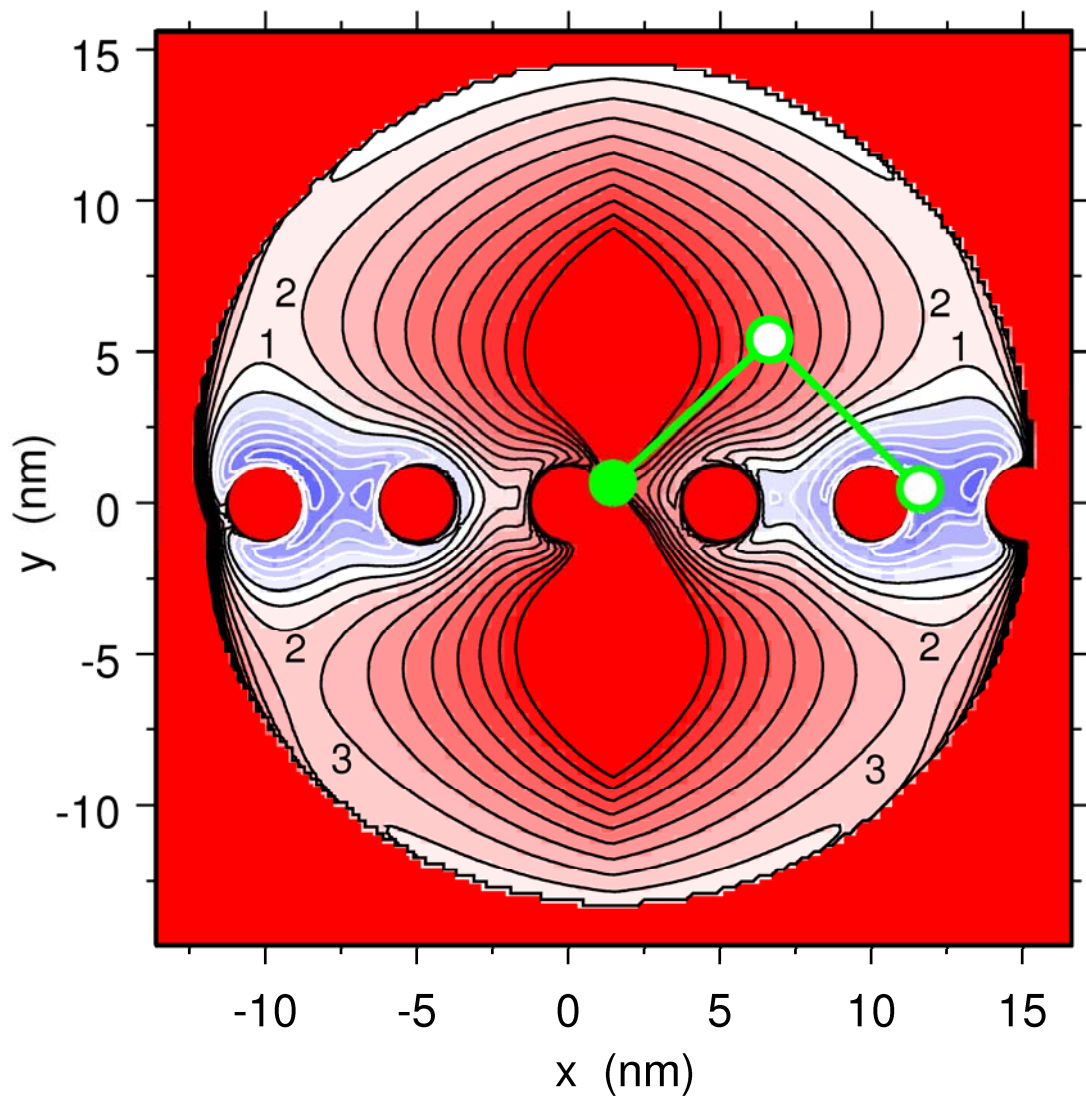


Figure S3 : Same as Fig. S2 but for protein bending rigidity $G = 4 k_B T$.

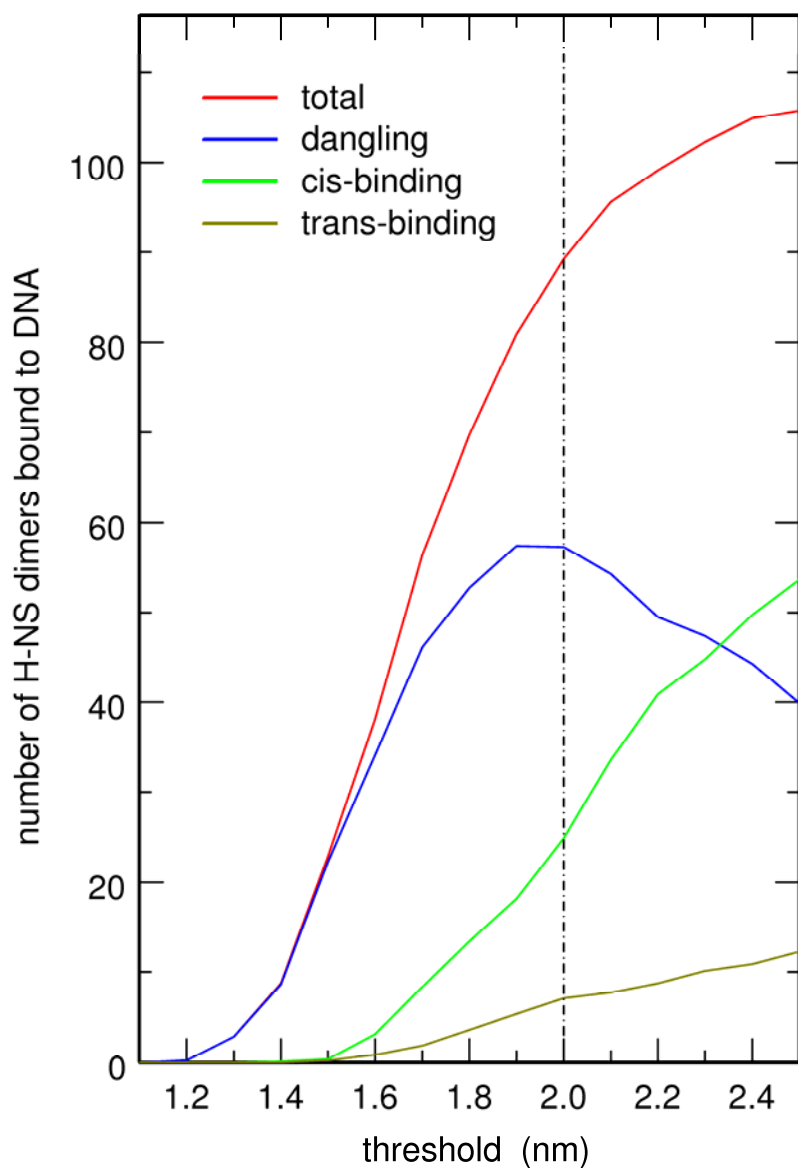


Figure S4 : Plot of the average number of H-NS dimers bound to DNA (red line), as well as the partition into dangling dimers (blue line), *cis*-binding dimers (green line), and *trans*-binding dimers (brown line), as a function of the threshold distance used to decide whether two beads are interacting together or not. Results presented in this paper were actually obtained with a 2.0 nm threshold (vertical dot-dashed line). This plot was computed from the conformations at final time (10 ms) for the eight 3D simulations with $G = 2 k_B T$.

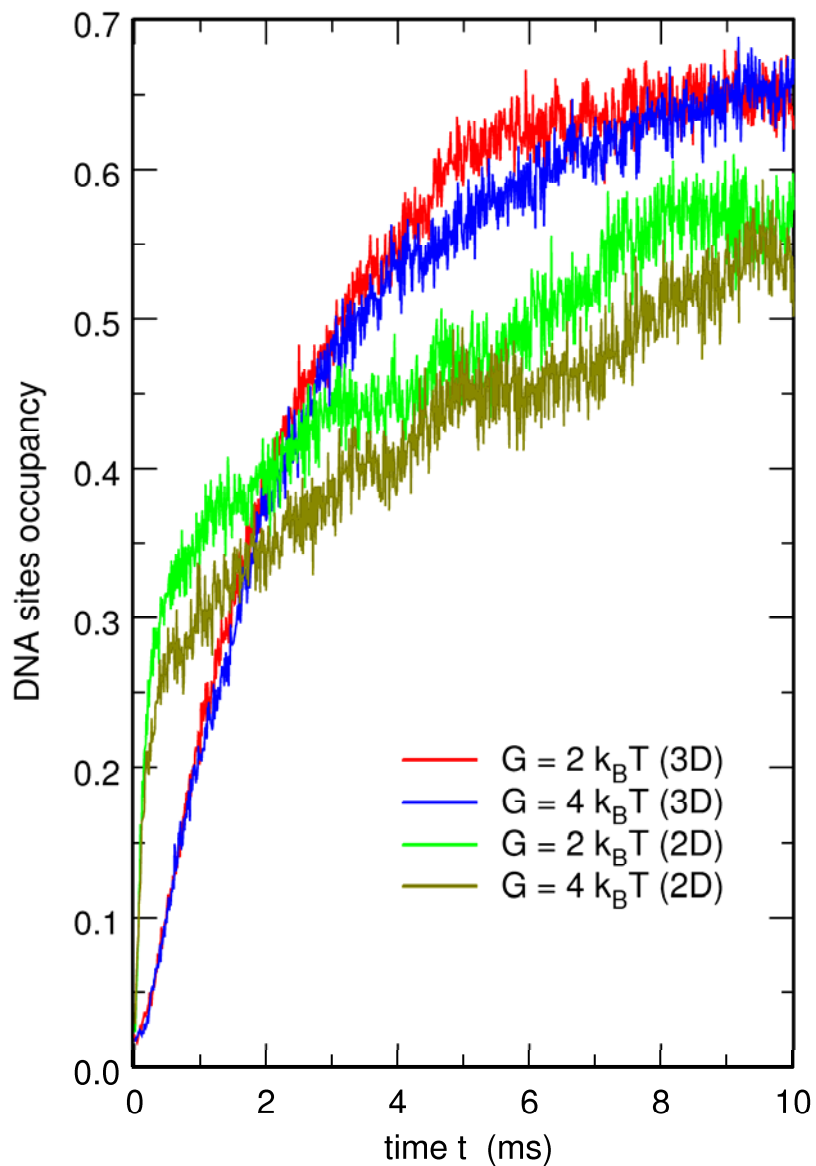


Figure S5 : Time evolution of the ratio of DNA sites bound to an H-NS dimer to the total number of DNA sites, for $G=2 k_B T$ and $G=4 k_B T$, and for 2D as well as 3D simulations. Note that the plasmid model contains 179 sites to which H-NS dimers can bind. 2D (respectively, 3D) results were averaged over 4 (respectively, 8) different trajectories.

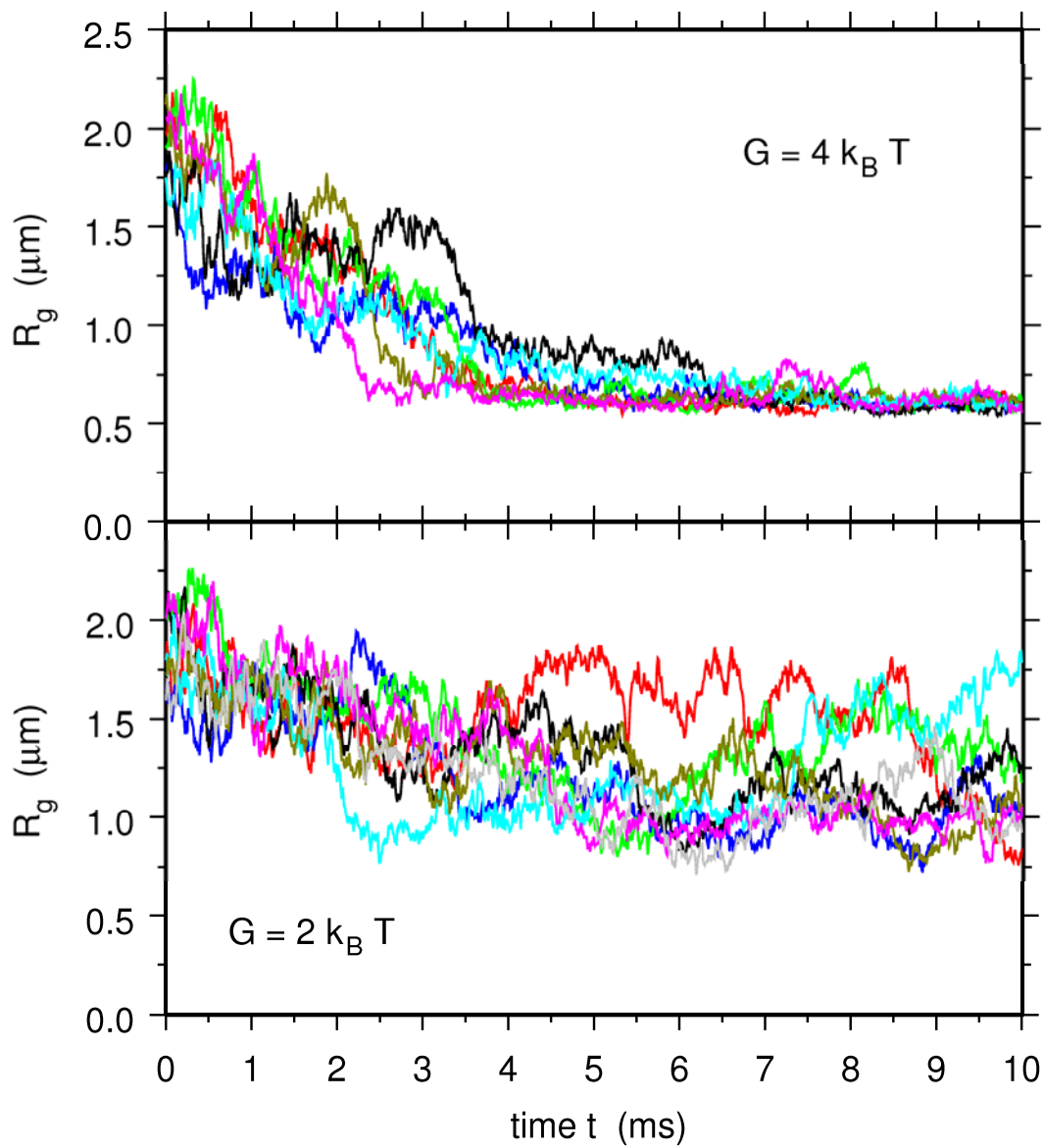


Figure S6 : The bottom and top plots show the time evolution of the radius of gyration of the plasmid molecule for eight simulations with $G = 2 k_B T$ and $G = 4 k_B T$, respectively.